Automated Multisensor Registration: Requirements and Techniques

Eric J.M. Rignot, Ronald Kowk, John C. Curlander, and *Shirley S. Pang*
Jet Propulsion Laboratory, California Institute of Technology, 4800 Oak Grove Drive, Pasadena, CA 91109

ABSTRACT: The synergistic utilization of data from a suite of remote sensors requires multi-dimensional analysis of the data. Prior to this analysis, processing is required to correct for the systematic geometric distortions characteristic of each sensor, followed by a registration operation to remove any residual offsets. Furthermore, to handle a large volume of data and high data rates, the registration process must be fully automated. A conceptual approach is presented that integrates a variety of registration techniques and selects the candidate algorithm based on certain performance criteria. The performance requirements for an operational algorithm are formulated given the spatially, temporally, and spectrally varying factors that influence the image characteristics and the science requirements of various applications. Several computational techniques are tested and their performance evaluated using a multisensor test data set assembled from the Landsat TM, Seasat, SIR-B, TIMS, and SPOT sensors. The results are discussed and recommendations for future studies are given.

INTRODUCTION

IN FUTURE YEARS a number of spaceborne remote sensing instruments for global monnitoring will become operational (NASA, 1987). These instruments will gather data over a broad range of the electromagnetic spectrum, allowing scientists to study the physical, chemical, and electrical properties of the Earth's environment on a global scale and over an extended period of time. To derive geophysical parameters of interest for each of the planned science applications, the data collected by these sensors must be combined and analyzed in a multidimensional manner. However, the sensors may be on different platforms and in different orbits, each having different physical characteristics, viewing geometries, and data collection and processing systems. Consequently, systematic and nonsystematic registration errors will exist between coincident multisensor data samples. It is a prerequisite for synergistic analysis of these data to estimate and correct for these errors.

Furthermore, because of the anticipated large data volume and high data rates of these future high resolution sensors, the traditional approach of visual identification of tiepoints to determine the deformation field is not an acceptable solution. It is necessary to develop an automated multisensor registration system that requires little or no operator supervision.

Although considerable experience has already been accumulated in the operational registration of Landsat data (IBM, 1978; Grebowsky, 1979; NASA, 1981), these techniques were designed to register multitemporal image data from passive sensors operating in the visible and near-visible part of the electromagnetic spectrum. These techniques are not well adapted to the registration of image data from multiple sensors of significantly different characteristics operating at different wavelengths. This paper specifically addresses the problem of developing a robust and adaptable automated multisensor registration technique that accomodates a wide variety of data types.

This paper is structured as follows. We first present a candidate set of performance requirements for development of an operational algorithm. These requirements are derived from the needs of several key science applications (Butler, 1984) as well as a review of practical limitations given the image characteristics. We then describe the multisensor test data set that has been assembled for evaluation of our registration algorithms. Several computational techniques that fit within this structure are tested. One technique uses high resolution digital elevation maps (DEM) of the areas to be registered. Others, which operate in the absence of ancillary data, are based on the extraction and matching of scene features across the different images to be coregistered. An assessment of each technique's performance is made using this multisensor test data set. The paper concludes with a discussion of the results and recommendations for future work.

PERFORMANCE REQUIREMENTS

CHARACTERIZATION OF THE INPUT DATA

A number of spatially, temporally, and spectrally varying factors influence the image characteristics and the registration accuracy.

The position and attitude of a sensor are usually known to some precision. The predicted image pixel location based on the knowledge of these platform parameters will result in an absolute location error. Similarly, uncertainty in the platform attitude will cause geometric distortion within an image frame. Depending on the stability of the platform and on the accuracy of estimate of the platform ephemeris and attitude, such errors can typically be removed by the use of tiepoints. However, nonsystematic errors and tiepointing errors result in a residual error in the image location and, therefore, a final step of refined image registration is necessary to obtain a sub-pixel level registration accuracy. Furthermore, we would prefer to eliminate any operator interactive tiepointing in the registration procedure.

Sensor specific geometric distortion of remotely sensed data may also result from the particular viewing geometry of the instrument. In the present of topography in the observed scene, perspective distortions are observed in off-nadir passive imaging. For an active sensor like a synthetic aperture radar (SAR), the terrain induced geometric distortions are quite different and are dominated by two phenomena: foreshortening and layover (Lewis and MacDonald, 1970). Rectification of these distortions is essential before registration of the data. As an illustration, a perspective view of geocoded and rectified multisensor imagery is shown in Figure 1 using a technique described by Kowk *et al.* (1987).

For sensors on different platforms and in different orbits, the acquired data are initially sampled to grids that are natural to the sensor geometry. A common grid for image coregistration, such as an Earth-fixed grid, is required. The process of mapping image data into this grid is known as geocoding and has been developed for a variety of sensors including SAR (Curlander *et al.*, 1987).

PHOTOGRAMMETRIC ENGINEERING & REMOTE SENSING,
Vol. 57, No. 8, August 1991, pp. 1029–1038.

0099-1112/91/5708–1029$03.00/0

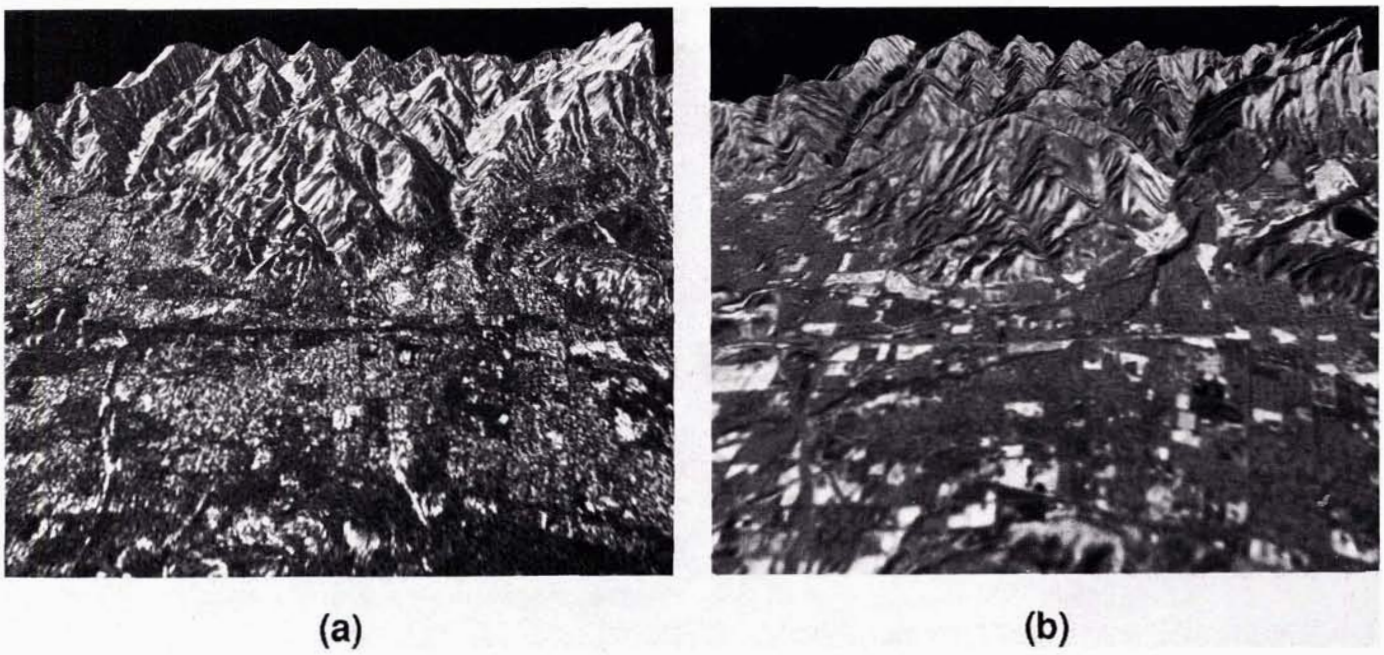

FIG. 1. Perspective views of multisensor geocoded and rectified images of an area near Los Angeles, California: (a) Seasat SAR image; (b) Landsat TM, Band 4, image.

The data collected by different sensors may also have significantly different spatial resolutions. As an example, the resolution of the suite of imaging sensors on the NASA Earth Observing System (EOS) platforms will range from tens of metres (SAR, HIRIS) to kilometres (MODIS, HMMR) (NASA, 1987). Because spatial resolution defines the ability of a system to discriminate objects within a scene, it establishes a limit for the achievable registration accuracy. Furthermore, depending on the range of spatial resolutions in the multisensor data to be coregistered, coarse to fine techniques of registration may be adaptively selected.

System noise (i.e., thermal noise, quantization noise, bit error noise, etc.) is another important factor affecting registration accuracy because many of the computational techniques used for registration are very sensitive to noise. While all sensors are corrupted by additive noise from the receiver electronics, SAR images are additionally corrupted by multiplicative noise known as image speckle. Thus, the multisensor registration techniques must be robust to a variety of noise sources of different statistical characteristics.

Finally, an additional consideration in any registration scheme is the scene composition. In cases where only a few features can be positive identified across the various sensors, the registration accuracy may be seriously impaired. Furthermore, identifiable features are inherently space, time, and frequency dependent. Therefore, it is necessary to develop robust automated techniques for selection of invariant features across the multisensor data.

In view of the above remarks, the input and output data requirements for an operational algorithm can be formulated. They define the operational domain and conditions under which the multisensor algorithm is expected to operate, and can be used as a basis for the evaluation of candidate algorithms.

Input Data Requirements

The input data are assumed to be corrected from the geometric distortions characteristic of each sensor using the best information available, geocoded onto a preselected grid common to all sensors (e.g., UTM), and resampled to the same pixel spacing. We further assume that the signal-to-noise ratio of the data is better than 5 dB, and the geodetic accuracy of the input images is better than 500 metres or 10 to 50 pixels (it is expected that most sensors will do better than this, given the accuracy of the available on-board positioning systems).

Output Data Requirements

The output products should have a registration accuracy better than one resolution element.

This requirement is derived from a subset of applications that are candidates for multisensor data analysis. Depending on the specific application, this accuracy requirement may be adjusted. For example, in the case of change detection, sub-pixel accuracy may be desired to compare the response of individual pixel elements. Depending on the scene characteristics (i.e., presence of identifiable features), this requirement may be indeed very difficult to achieve. In other cases, such as the global study of hydrological cycles (which includes tasks such as sea-ice identification and dynamics, determination of moisture content of soil and vegetation, vegetation identification, areal extent and growth, etc.), a registration of accuracy of several hundred metres may be sufficient.

It is important to point out that, although the accuracy requirements have typically been well defined for each individual instrument, little or no accuracy requirements have yet been clearly defined for multisensor registration by the scientific community. More work is clearly needed in this area for each interdisciplinary science application.

MULTISENSOR TEST DATA

A multisensor test data set has been assembled using image products from Seasat SAR, SIR-B, Landsat TM, SPOT, and TIMS (Kwok *et al.*, 1989). Information on each sensor-including look angle, spectral range, polarization, and spatial resolution-is given in Table 1. Geocoding of the images to a common UTM Earth-grid has been performed and the data have resampled to the same pixel spacing of 25 metres. Several sub-images of reduced

size (512 by 512, 1024 by 1024 pixels) were selected from the areas where the sensors have coincident coverage. The characteristics of the original image data and of the selected sub-images are presented in Table 2. This table includes information about the geographic location of the data, the initial sample spacing and size, the revolution number and date of acquisition, the number of selected sub-images, and the type of map projection used for coding. A summary list of the natural features present in the imaged scenes is also indicated.

For each selected sub-image, manual registration was performed, resulting in an estimated relative misregistration uncertainty of less than ± 2 pixels, roughly equal to the largest

TABLE 1. DESCRIPTION OF THE CHARACTERISTICS OF THE DIFFERENT SENSORS INVOLVED IN THE CONSTITUTION OF THE MULTISENSOR TEST DATA SET.

NAME OF SENSOR	TYPE	FREQUENCY	RESOLUTION (ORIGINAL DATA)
SEASAT	SAR ACTIVE	L BAND, HH POLARIZATION 23 ° LOOK-ANGLE	25 m
SIR-B	SAR ACTIVE	L BAND, HH POLARIZATION 15 TO 60 ° LOOK-ANGLE	25 m
TIMS	RADIOMETER PASSIVE	THERMAL-INFRARED	30 m
LANDSAT TM	OPTICAL PASSIVE	7 BANDS SPECTRAL RANGE: 1 .45 µm - .52 µm; 2 .52 µm - .60 µm; 3 .63 µm - .69 µm; 4 .76 µm - .90 µm; 5 1.55 µm - 1.75 µm; 6 1.04 µm - 1.25 µm; 7 2.08 µm - 2.35 µm	28.5 m (pixel spacing) IFOV
SPOT	OPTICAL PASSIVE	3 BANDS SPECTRAL RANGE: 1 .50 µm - .59 µm; 2 .61 µm - .68 µm; 3 .79 µm - .89 µm	20 m (pixel spacing) IFOV

TABLE 2. DESCRIPTION OF THE MULTISENSOR TEST DATA SET.

IMAGE FRAMES LOCATION	SEASAT	LANDSAT	SPOT	TIMS	FEATURES IN PATCHES
ALTAMAHA RIVER, GEORGIA (pixel size = 20 m)	Rev : 407 Date: Jul 78 Size: 5 K x 5 K Map Proj. : UTM # of patches selected for testing: 12	Date: Jul 84 Size: 3 K x 4 K Rotated to North # of patches selected for testing: 12	Date: Sept 84 Size: 3 K x 5 K Rotated to North # of patches selected for testing: 12		Rivers, Lakes, Fields, Roads, Coasts.
WIND RIVER BASIN, WYOMING (pixel size = 30 m)	Rev : 781 Date: Aug 78 Size: 5 K x 5 K Map Proj. : UTM # of patches selected for testing: 5	Date: Jun 84 Size: 5 K x 5 K Rotated to North # of patches selected for testing: 13			Mountains, Rivers, Lakes, Fields, Roads, Cities,
YUMA, ARIZONA (pixel size = 25 m)	Rev : 681 Date: Aug 78 Size: 3 K x 3 K Map Proj. : UTM # of patches selected for testing: 13	Date: Jun 84 Size: 3 K x 4 K Rotated to North # of patches selected for testing: 13			Mountains, Rivers, Fields, Roads, Cities, Dunes.
DEATH VALLEY, CALIFORNIA (pixel size = 25 m)	Rev : 882 Date: Aug 78 Size: 5 K x 5 K Map Proj. : UTM # of patches selected for testing: 4	Date: Nov 82 Size: 3 K x 4 K Rotated to North # of patches selected for testing: 4		Date: Jul 83 Size: 1 K x 1 K Rotated to North # of patches selected for testing: 4	Mountains, Fields.

resolution element (40 metres). This uncertainty results primarily from the differences in resolution between the various sensors. This estimate is used as a basis for the true registration to evaluate the performance of the various automated registration techniques.

AUTOMATED MULTISENSOR REGISTRATION

The structure of the candidate multisensor registration algorithms is presented in Figure 2. The input data satisfy the requirements as formulated in the previous section. The first processing step consists of automatically selecting sub-frames from each input image to define local areas of multisensor coincident coverage where precision registration can be performed with a high confidence of success. Depending on the availability of ancillary data (DEM or topographic maps), a registration mode is selected. For the case where a DEM is available, the multisensor data are coregistered to the common grid provided by the DEM. Otherwise, invariant features are extracted from the sub-images and correspondence is established across the data to be registered. To reduce the computational complexity of the algorithm and obtain several estimates of the misregistration per sub-image, feature matching is performed at multiple locations and the results are then filtered to evaluate their relative spatial consistency within the selected patch (local constraints). If the match can be labeled as statistically significant (e.g., satisfies some goodness measure), the misregistration error of the selected sub-image is estimated and the multisensor data are then registered. Otherwise, the result is rejected and the selection and matching process is repeated with different parameters. At a higher level of processing, the combined results from different features and from registered neighborhood patches can be used to produce a more accurate and more reliable solution. In effect, a cooperative process can be established where the results from different stages of the processing are used as reinforcements for the entire process.

Several candidate techniques which are effective within this structure are presented in the remainder of this section. They have been selected based on compatibility, robustness, and adaptivity to the various sensors. Each matching algorithms' performance is assessed using the multisensor test data set described in the last section.

Automated Selection of Sub-Images

Selection of the patches where fine registration is desired must be based on the extraction of stable features that can be unambiguously identified across the entire multisensor image data set. Candidate features include rivers, lakes, coast-lines, roads, or scene-dominant man-made or natural structures. One possible technique was desribed in Davis and Kenue (1978) where binary edge maps were used to compute a figure of merit for candidate control points. The results obtained with images from different sensors are then cross correlated to retain valid candidates.

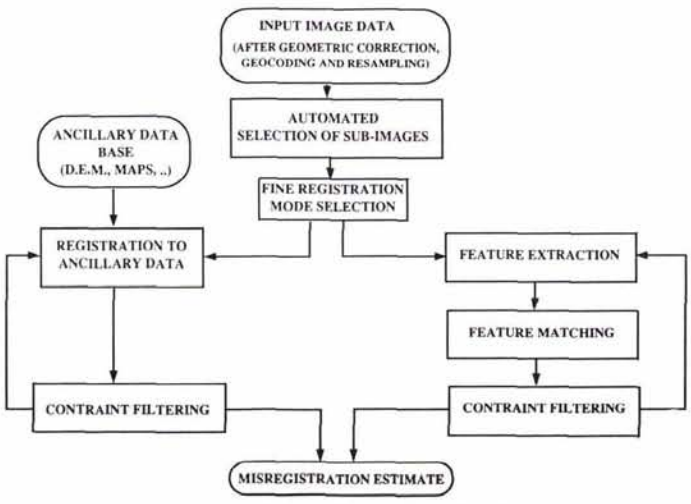

FIG. 2. Flow chart of the multisensor registration algorithm.

Automated Registration to Digital Terrain Data

Our approach is to simulate multisensor imagery from a digital elevation map (DEM) of the area where the sensors have a coincident coverage and register this simulated imagery with the actual imagery, thereby inducing coregistration of the multisensor data on the common grid provided by the DEM.

Using elevation data, viewing geometry, and a model of the scene reflectance, the appearance of the scene for any given sun angle and viewing angle can be simulated as in Horn and Bachman (1978), Woodham (1980), Little (1980), and Frew (1984) for passive sensors operating in the visible and near-visible part of the spectrum. An example of a simulated image generated using this technique is shown in Figure 3. The illumination parameters were matched to Landsat TM image data acquired over the same area. A qualitative sense of how well the simulated image predicts the real image can be obtained by visually comparing the two figures. A simple matching technique (area-correlation) is then used to establish the correspondence between the images. Visual tiepointing of identifiable features in areas away from the registered images was performed to assess errors in the registration. The registration error is approximately 80 metres for the images shown. A more elaborate matching scheme using features derived from the simulated and actual imagery was proposed by Little (1980); however, no error analysis was performed.

Our approach to generate simulated SAR image from the DEM is similar to that described above. The sensor imaging geometry, the elevation data, and a model of the radar backscatter are all required to produce the image shown in Figure 4 (Kwok *et al.*, 1989). The imaging geometry simulates that of a Seasat image acquired over the same area. Except for the speckle noise which is apparent in the actual image, the geometry of the simulated data appears identical to the actual image. An area correlation scheme is then used to match the radar and simulated images. Using tiepoint measurements of identifiable features not within the image shown, a misregistration error of 60 metres was obtained. Again, more elaborate schemes to select ground points most probable for matching could be implemented to optimize this procedure.

Several potential error sources affect the registration accuracy. First is the uncertainty in the actual imaging geometry which causes geometric distortion in the simulated image relative to the actual image. Second is the geometric accuracy of the DEM data. In both cases, the simulation of the radiometric (incidence angle calculations) and the geometric distortions are dependent on the absolute and relative height accuracies. The terrain data used for the simulation were digitized from existing topographic maps with 50 metre contour intervals. Thus, there are digitization errors as well as sampling errors associated with each digital elevation sample point. Higher quality elevation data derived from aerial photographs (e.g., from USGS 24,000-scale maps) may be more appropriate for image data with the resolutions of HIRIS, SAR, or SPOT. A third error source results from the reflectance model used for the visible wavelength data and the absence of atmospheric attenuation effects.

Computational Approaches

In the absence of reference maps, elevation data, geographical information, or correlative ground truth information, blind

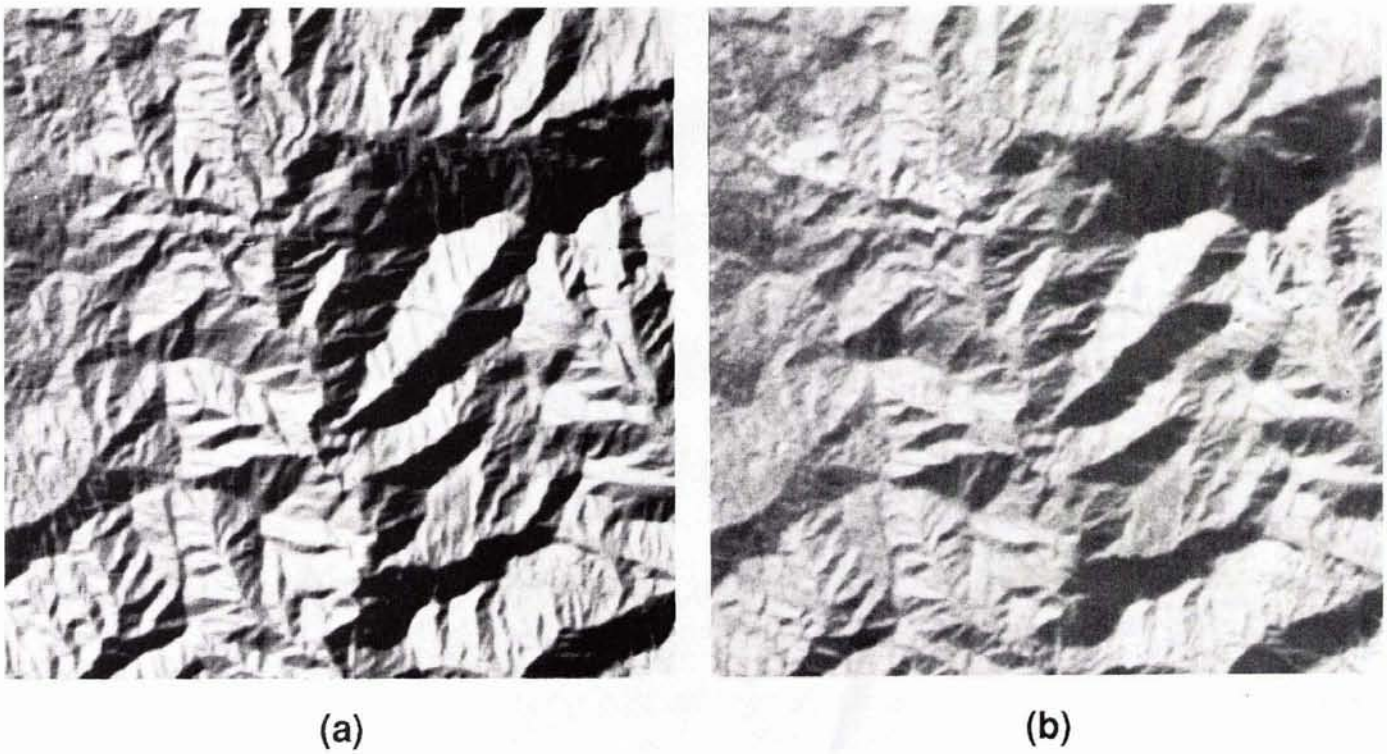

FIG. 3. Comparison of simulated versus actual Landsat TM image: (a) simulated image; (b) actual image.

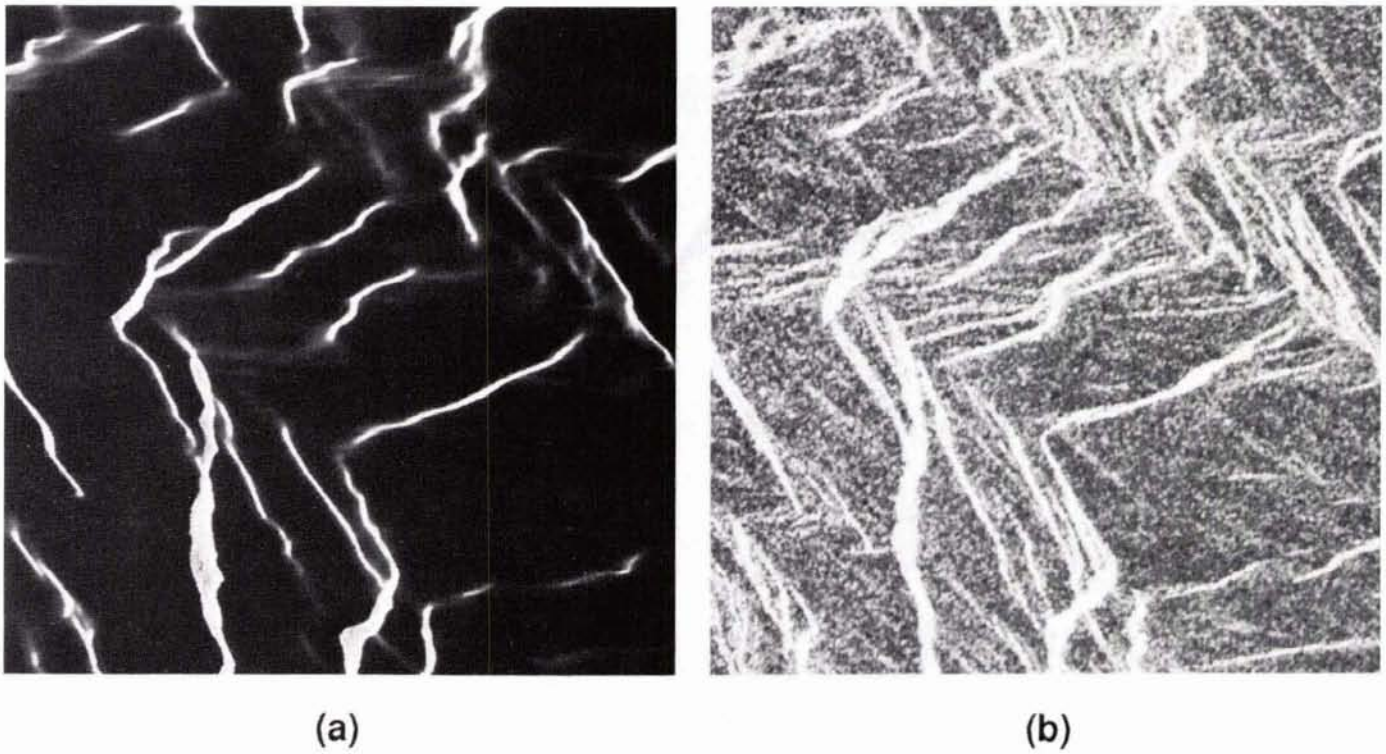

FIG. 4. Comparison of simulated versus actual Seasat SAR image; (a) simulated image; (b) actual image.

techniques based on the identification of invariant features across the data can be used for image registration. Several candidate techniques which are effective within the structure of our algorithm are presented in this section. Their performance is assessed and compared using the multisensor test data set.

Feature Extraction

Candidate features commonly used in digital imagery include edges, regions, lines, vertices of line intersection, shapes, etc. These features must be robust to change in sensor geometry, wavelength, signal-to-noise ratio (SNR), and noise statistics. Two particular types of features—region boundaries and edges—were examined using our multisensor data set. The result of the corresponding segmentation techniques are discussed next.

Multisensor Region Boundary Extraction

The brightness response (i.e., reflectance, thermal signature, backscatter coefficient, etc.) of a homogeneous area (or region) depends on multiple parameters, such as look angle, frequency, polarization, physical and electrical characteristics of the surface, chemical composition, meteorological conditions, etc. As a result, it may vary considerably from one instrument to another, rendering impractical techniques based on region brightness cross correlation. However, the shape, spatial extent, or location in the image plane of regions of similar homogeneous statistical properties may still be largely preserved across multisensor data. Region boundaries are probably the simplest low-level features that can be used to characterize the misregistration.

Even though many unsupervised segmentation techniques exist for optical images, most of them are not effective for SAR images because of the presence of speckle noise. One unsupervised technique that seems to work reasonably well is a scheme based on a clustering algorithm to segment the images into several regions of similar intensity and texture (Kwok *et. al.*, 1989). The region boundaries are then established where a class transition occurs.

The resulting segmentation map, using three classes, is shown in Figure 5 together with the original images from Seasat, Landsat, and SPOT. A 3- by 3-pixel window was used at each pixel location to compute the mean grey level and grey level texture by means of a simple standard deviation measure. Larger windows produce more homogeneous regions with smoother boundaries but decrease the localization accuracy of the boundary elements. The results obtained by matching these region boundaries are usually less accurate than those obtained with other techniques. However, region segmentation can still be refined, especially in the case of SAR imagery, to provide information that complements results from other techniques.

Multisensor Edge Detection

Extensive literature exists on the subject of edge detection in optical imagery. However, in the case of SAR images the detection process is complicated because the images are corrupted by speckle noise. Techniques based on an approximation of the first and second directional derivatives, (e.g., Sobel or Robert operators) perform poorly, especially in terms of localization of the edges because they tend to produce large responses. Statistical edge operators such as those by Touzi *et al.* (1988) and Frost *et al.* (1982) in a lot of cases suffer from the same limitation.

This problem is solved by regularization techniques, specifically using a two-dimensional Gaussian smoothing operator such as a Marr-Hildreth operator (Marr and Hildreth, 1980) or a Canny edge detector (Canny, 1986). These operators have (1) good detection properties, (2) good localization properties, and (3) no multiple responses to a single edge, the three performance criteria for evaluation of edge detection algorithms. In the Marr-Hildreth approach, the edges are marked at the zero-crossings of the Laplacian of a Gaussian-smoothed image. In the Canny operator they are marked at the maxima of the gradient magnitude of the Gaussian-smoothed image. The detector is a simple approximation to an optimal operator and is based on an optimization between the three aforementioned criteria of good detection. Theoretically, these techniques are compatible with almost all types of remote sensor data. Their performance with optical data have been documented in the literature (Marr and Hildreth, 1980; Canny, 1986).

The performance of these two operators was quantitatively compared in Kwok and Rignot (1989) for the case of synthetic SAR images as well as actual SAR images. It was shown that the gradient operator outperforms the Laplacian operator in both detection and localization of edges in image speckle, thus illustrating that the Marr-Hildreth operator is sensitive to high spatial frequencies such as produced by speckle noise, whereas the directional gradient remains fairly robust.

Significant improvements in the performance of the ∇G operator can result from optimizing the parameter selection (Kwok, *et al.*, 1989). In particular, the value of the filter spatial width σ must be adapted to the spatial resolution of the different sensors. Typically, the smallest width compatible with the spatial resolution produces the best results. Automatic thresholding is another important factor. However, because no *a priori* information about the actual presence, location, and strength of edges in the imaged scene is available, an optimal strategy is difficult to establish. In our implementation, a threshold with hysteresis (Canny, 1983) is used to eliminate insignificant edges. Because the gradient magnitude distribution varies with the sensor (e.g., Gaussian distribution for an optical image and Rayleigh distribution for a SAR image), the threshold values need to be adaptable. Good results were obtained when the thresholds were set based on the computed mean and the standard deviation of the gradient magnitude.

Further post-processing such as thinning and contour-filling techniques have been shown in Kwok *et al.* (1989) to improve the quality of subsequent matches. Another possible improvement of the edge detector uses multiple operator widths and combines the resulting edges using a technique called feature synthesis, where the responses of the smaller operators are used to predict the response of a large operator. Results with optical images have been presented by Canny (1983) where it was noted that most of the edges are actually determined by the smaller operator.

For illustration, one example of edge-map using Seasat, Landsat TM and SPOT data and the Canny edge detector with a spatial width of 2 pixels (40 m) and adaptive thresholding is presented in Figure 6.

Feature Matching

Candidate feature matching techniques include binary cross correlation, distance transform and Chamfer matching, dynamic programming, and structural or symbolic matching.

In the case of region boundaries and edges, a convenient binary representation of the feature maps can be used: a grey level of one at location of a feature point and zero otherwise. This representation reduces the computational complexity of feature matching because computational cost becomes proportional to a linear dimension as opposed to area correlation where computational cost is proportional to an area.

Binary Correlation

The binary feature maps of each of the images to be registered can be cross correlated for various relative image shifts. The shift corresponding to the peak of the cross correlation will be an estimate of the actual misregistration between the images. The process is fast and can be efficiently implemented on an array processor or vectorizing computer.

Distance Transform and Chamfer Matching

The distance transform and Chamfer matching techniques are described in Barrow *et al.* (1977). In this method feature points are matched by minimizing a generalized distance between them.

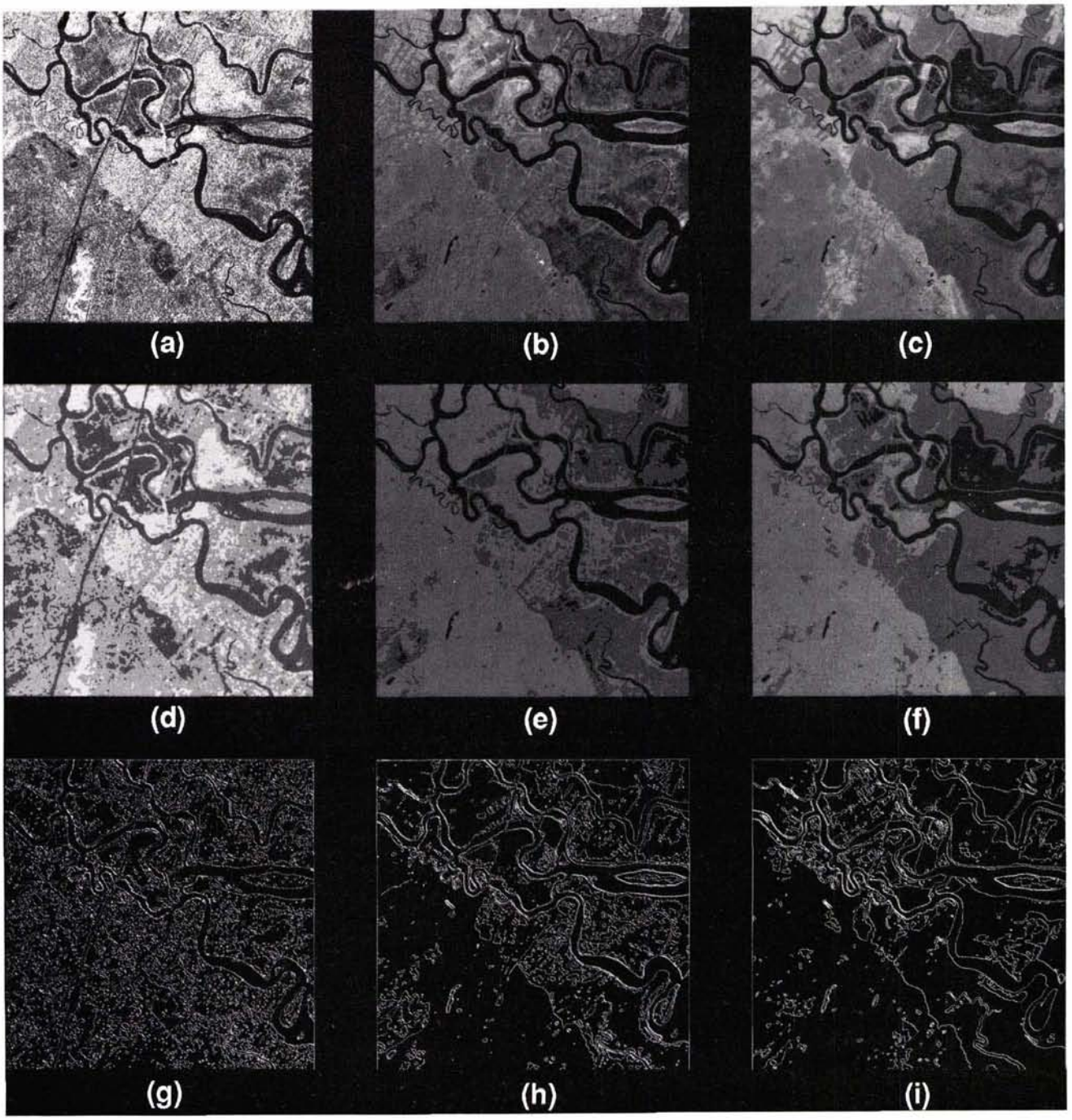

FIG. 5. Unsupervised segmentation of optical and SAR images from an area near the Altamaha River, Georgia. (a) Seasat, (b) Landsat TM, and (c) SPOT images are segmented into three regions represented in (d), (e), and (f), respectively. The corresponding images of region boundaries are (g), (h), and (i), respectively.

A distance transform is first applied to a binary feature map, arbitrarily referred to as the source image. The result of this transformation is a distance map where the grey level of each pixel is a measure of the distance between the pixel and the nearest feature point. For various values of the relative shift between the source and the target images, the total distance between the feature points of the two images can be computed. This measure is the sum of the distance values read from the source image at each location of a feature point in the target image. If matching were perfect, this distance would be zero. The relative shift that produces the smallest total distance corresponds to an estimate of the actual relative misregistration between the images to be registered.

This method is more robust to distortion or residual rotation effects than a binary correlation method.

COMPARISON OF BINARY CORRELATION AND CHAMFER MATCHING

A comparison of the performance of the two techniques has lead to the following observations.

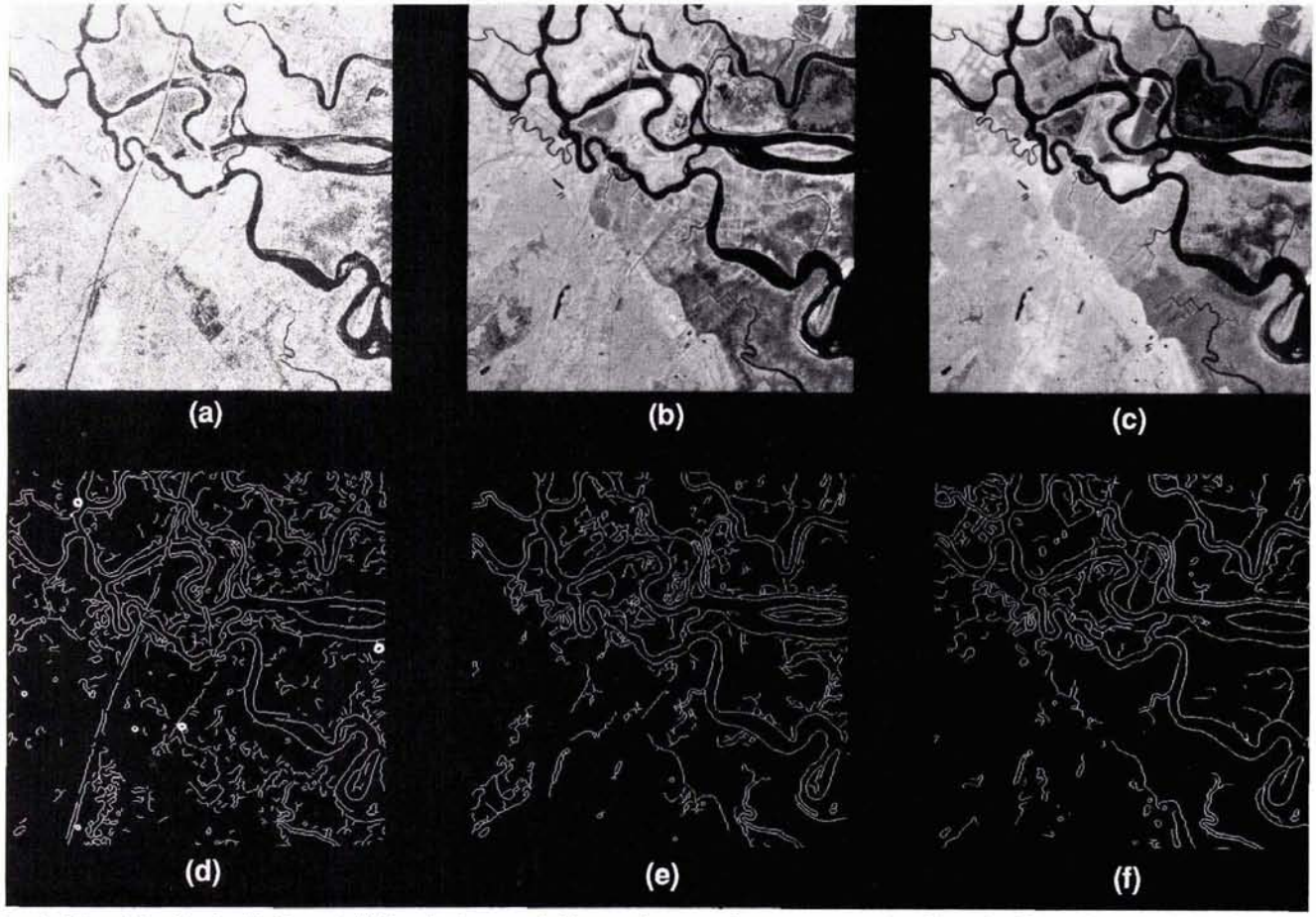

FIG. 6. Edge detection in (a) Seasat, (b) Landsat TM, and (c) SPOT images of an area near the Altamaha River, Georgia. The edge-maps obtained from Canny's edge detector are represented in (d), (e), and (f), respectively.

The time of computation of the binary correlation is less than the time of computation of Chamfer matching, typically in the ratio 1 to 4 for a search area of 100 by 100 pixels using a 512 by 512 pixel image.

The tolerance to residual rotation effects is 1 degree in the case of the binary cross correlation based on a maximum registration accuracy of 2 pixels. This tolerance is improved to 3 degrees when thicker edges are used (e.g., 3 pixels) (Wong, 1977). In the case of Chamfer matching the rotation tolerance is 3 degrees.

Better registration results (10 to 20 percent) were consistently obtained by binary correlation as compared to Chamfer matching. The reason is that the quality metric used during Chamfer matching does not perform as well as expected with multisensor data due to the presence of non-matchable edges across the data, i.e., edges that appear in one image and not in the other. Their presence biases the total distance between feature points and significantly affects the accuracy, whereas the binary cross correlation is not affected by non-matchable edges.

DYNAMIC PROGRAMMING

This iterative method, combined with an autoregressive model (AR), was used in this work by Maitre and Wu (1989) to register severely distorted optical images to a reference map without *a priori* knowledge of the distortion. The two processes work at different levels. At the lower level, dynamic programming optimizes the search for best registration of an ordered set of features (e.g., edges) extracted from the source image with a comparable set of features extracted from the reference map. At a higher level, the AR model defines the deformation of the image at a pixel scale. The technique is robust to non-matchable edges and good results are shown in Maitre and Wu (1989) using NOAA-7 satellite data.

This method has not yet been tested using our multisensor test data set, but offers good potential. A simpler deformation model could be used for fine registration of multisensor data. One limitation is the complexity of the process, which is proportional to the number of feature points (typically several thousand are required in practical applications). Additionally, the process would be difficult to implement on a parallel machine because feature points are tracked sequentially.

Constraint Filtering

In practice, matching is performed on small areas to minimize the distortion. Thus, the time of computation is also reduced and the number of independent estimates of the misregistration between the two images is increased. The resulting data must therefore be filtered to eliminate false matches. A clustering technique can be used where the cluster centroid corresponds to the estimated misregistration of the images. For our test dataset, the 512- by 512-pixel patches extracted from actual multisensor images were divided into four sub-patches of size 256 by 256. When three or four local shifts were consistent (i.e., within $\pm$ 4 pixels), the match was assumed correct and the mean of the resulting cluster of the consistent sub-patches defined our estimate of the global shift. Otherwise, matching was

assumed incorrect and the segmentation was repeated with different parameters or other features were used in the original segmented image.

A more robust approach would combine results obtained from various low level processing techniques. A number of techniques could be cooperatively combined to improve clustering of the data. Results from neighborhood patches could also be included.

EXPERIMENTAL RESULTS

The expected relative shift of each pair of images is zero with an uncertainty typically of ± 2 pixels. If we assume normally distributed zero-mean error sources,

$$\sigma_{\text{Actual}} = \sqrt{\sigma^2_{\text{Algo}} - \sigma^2_{\text{Meas}}}$$

where σ_{Actual} is the actual standard deviation of the registration error, σ_{Algo} is the standard deviation of the shift estimation error by the algorithm, and σ_{Meas} is the standard deviation of the manual registration error. For a measurement error of 2 pixels, knowing that $\sigma_{\text{Algo}} \approx 3$ pixels, we determine the standard deviation of the registration error to be of 2 pixels.

Twelve 512- by 512-pixel images corresponding to three different geographic areas were registered. Each image was divided into four sub-blocks, and the search area for the local registration shift was 101 by 101 pixels in each sub-block, corresponding to a maximum expected shift of 50 pixels both along the vertical and along the horizontal directions.

Using a binary correlation of edges, Seasat and SPOT images were coregistered with a rate of success of 87 percent before constraint filtering and 92 percent after, and no false matches. Using the same technique, Seasat and Landsat TM images were coregistered with a rate of success of 85 percent before constraint filtering, and 86 percent after. Registration was qualitatively more difficult in that latter case because of the lower resolution of the Landsat images as compared to SPOT images, and also because a few additional scenes whose content made registration more difficult were used.

The achievability of sub-pixel accuracy seemed difficult to establish by visual inspection of our multisensor test data set. This is certainly a limiting factor when comparing digital imagery from multiple remote sensors.

CONCLUSIONS AND RECOMMENDATIONS

With the advent of an era of diverse sets of remote sensors on common platforms (e.g., EOS), it is of considerable importance to develop automated multisensor registration tools for synergistic use of the data. A high level algorithm for multisensor registration that integrates a variety of techniques in a systematic manner was discussed in this paper. Low level techniques used by this algorithm were tested using a limited multisensor data set. A more complete study would require that this data set be enlarged to include more instruments and more scene types, and that the performance of additional feature extraction and feature matching techniques be evaluated.

We insisted that the performance of a multisensor registration algorithm is dependent on application specific science requirements as well as on the instrument characteristics, the nature and composition of the imaged surface, and the environmental conditions. The task of automated multisensor registration was described as very complex and not solvable using a single technique. It requires the combination of multiple techniques that work in a competitive-cooperative mode of interaction. For this reason, a rule-based artifical intelligence approach may be necessary for a more advanced high-level algorithm to automatically select optimal techniques and parameters from a particular multisensor application.

ACKNOWLEDGMENTS

The authors wish to thank R. Fätland for his contributions to the software development effort and A. Pang and J. Weirick for their data processing support. This work was carried out under contract with the National Aeronautics and Space Administration at the Jet Propulsion Laboratory, California Institute of Technology.

REFERENCES

Barrow, H. G., J. M. Tenenbaum, R. Bolles, and H. C. Wolf, 1977. Parametric Correspondence and Chamfer Matching: Two New Techniques for Image Matching. *Proc. 5th Joint Conf. on Artificial Intelligence*, Cambridge, Mass., 1977, pp. 659–663.

Butler, D., author, author, and author, 1984, *Earth Observing System: Science and Mission Requirements Working Group Report*, Vol. I, NASA TM 86129, 51 p.

Canny, J. F., 1986. A Computational Approach to Edge Detection. *IEEE Trans. on Pattern Anal. and Mach. Intell.*, Vol. 8, No. 6, pp. 679–698.

Canny, J. F., 1983. *Finding Edges and Lines in Images*. Artif. Intell. Lab., Mass. Inst. Technol., Cambridge, Mass., Tech Rep. AI-TR-720.

Curlander, J. C., R. Kwok, and S. Pang, 1987. A Post-Processing System for Automated Rectification and Registration of spaceborne SAR Imagery, *Int. Journal of Remote Sensing*, Vol. 8, No. 4, pp. 621–638.

Davis, W. A., and S. K. Kenue, 1978. Automatic Selection of Control Points for the Registration of Digital Images, *Proc. of the Int. Joint Conference on Pattern Recognition, 4th*, Kyoto, Japan, 7-10 Nov 1978, pp. 936–938.

Frew, J., 1984. Registering Thematic Mapper Imagery to Digital Elevation Models, *Machine Processing of Remotely Sensed Data Proceedings*, pp. 191–195.

Frost V. S., K. S. Shanmugan, and J. C. Holtzman, 1982. Edge Detection for Synthetic Aperture Radar and other Noisy Images. *Digest from the Intl. Geoscience and Remote Sensing Symposium*, FA-2, p. 4.

Grebowsky, G. J., 1979. Lacie Registration Processing, *The LACIE Symposium, Proceedings of the Technical Sessions*, July 1979, pp. 87–97.

Horn, B. K. P., and B. L. Bachman, 1978. Using Synthetic Images to Register Real Images with Surface Models, *Comm. ACM*, Vol. 21, pp. 914–924.

IBM, 1978. *MSS Data Processing Description*, IBM Federal Systems Division Report, Contract NAS5-22999.

Kwok, R., J. C. Curlander, and S. Pang, 1987. Rectification of Terrain Induced Distortion in Radar Imagery, *Photogrammetric Engineering & Remote Sensing*, Vol. 53, No. 5, pp. 507–513.

Kwok, R., and E. Rignot, 1989. *Comparison of the $\nabla^2 G$ and ∇G Operators for Edge Detection in Speckle Noise* (in preparation).

Kwok, R., E. Rignot, J. C. Curlander, and S. Pang, 1989. *Multisensor Image Registration: A Progress Report*, Jet Propulsion Laboratory Internal Report JPL D-6697.

Lewis, A. J., and H. C. Mac Donald, 1970. Interpretive and Mosaicking Problems of SLAR Imagery, Remote Sens. Environ., 1, 213–218.

Little, J. J., 1980. Automatic Rectification of Landsat Images using Features derived from Digital Terrain Models, Univ. of British Columbia. Tech. Rep. 80–10.

Maitre, H., and Wu, Y., 1989. Dynamic Programming Algorithm for Elastic Registration of Distorted Pictures based on Autoregressive Model, IEEE Trans. on Acoust., Speech, and Sign. Proc., 37, 2, 288–297.

Marr, D., and E. Hildreth, 1980. Theory of Edge Detection. Proc. Royal Soc. London, B, 207, 187–217.

IBM, 1978. *MSS Data Processing Description*, IBM Federal Systems Division Report, Contract NAS5-22999.

NASA, 1981. *ERSYS Registration Subsystem Detailed Design Specification*, AgRISTARS Report SR-I1-04154, Contract NAS9-14350, JSC No. 16946.

NASA, 1987. *EOS Earth Observing System Reports*, NASA Techn. Memorandum 86129, Vol. I and Vol. II, NASA Publish.

Touzi, R., A. Lopes, and P. Bousquet, 1988. A Statistical and Geo-

metrical Edge Detector of SAR Images. *IEEE Trans. Geosci. and Remote Sens.*, Vol. 26, No. 6, pp. 826–831.

Ulaby, F., R. K. Moore, and A. K. Fung, 1986. *Microwave Remote Sensing: Active and Passive III*, Artech House Inc., Norwood, Mass.

Wong, Y. R., 1978. Sequential Scene Matching using Edge Features. *IEEE Trans. on Aerospace and Elect. Systems*, Vol. 14, No. 1, pp. 128–140.

Woodham, R. J., 1980. Using Digital Terrain Data to Model Image Formation in Remote Sensing, *SPIE, Image Processing for Missile Guidance*, Vol. 238, pp. 75–78.

(Received 13 July 1990; accepted 13 September 1990; revised 16 October 1990)

Forthcoming Articles

Eugenia M. Barnaba, Warren R. Philipson, Arlynn W. Ingram, and *Jim Pim,* The Use of Aerial Photographs in County Inventories of Waste-Disposal Sites.

Michel Boulianne, Louis Cloutier, and *Sanjib K. Ghosh,* Cerebral Biopsies Using a Photogrammetric Probe Simulator.

Haluk Cetin and *Donald W. Levandowski,* Interactive Classification and Mapping of Multi-Dimensional Remotely Sensed Data Using n-Dimensional Probability Density Functions (nPDF).

Yue Hong Chou, Slope-Line Detection in a Vector-Based GIS.

Raymond L. Czaplewski, Misclassification Bias in Areal Estimates.

Heinrich Ebner, Wolfgang Kornus, Gunter Strunz, Otto Hofmann, and *Franz Muller,* A Simulation Study on Point Determination Using MOMS-02/D2 Imagery.

Peter F. Fisher, First Experiments in Viewshed Uncertainty: The Accuracy of the Viewshed Area.

Peter F. Fisher, First Experiments in Viewshed Uncertainty: Simulating Fuzzy Viewsheds.

G. M. Foody, A Fuzzy Sets Approach to the Representation of Vegetation Continua from Remotely Sensed Data: An Example from Lowland Heath.

W. Frobin and *E. Hierholzer,* Video Rasterstereography: A Method for On-Line Measurement of Body Surfaces.

Peng Gong and *J. Douglas Dunlop,* Comments on the Skidmore and Turner Supervised Nonparametric Classifier (and response).

Daniel K. Gordon, Paul W. Mueller, and *Matthew Heric,* An Analysis of TIMS Imagery for the Identification of Manmade Objects.

Peter E. Joria, Sean C. Ahearn, and *Michael Conner,* A Comparison of the SPOT and Landsat Thematic Mapper Satellite Systems for Detecting Gypsy Moth Defoliation in Michigan.

D. King, Determination and Reduction of Cover Type Brightness Variations with View Angle in Airborne Multispectral Video Imagery.

J. Lavreau, De-Hazing Landsat Thematic Mapper Images.

Zhilin Li, Effects of Check Points on the Reliability of DTM Accuracy Estimates Obtained from Experimental Tests.

Donald L. Light, The New Camera Calibration System at the U. S. Geological Survey.

Hans-Gerd Maas, Digital Photogrammetry for Determination of Tracer Particle Coordinates in Turbulent Flow Research.

Ronald T. Marple and *Eugene S. Schweig, III,* Remote Sensing of Alluvial Terrain in a Humid, Tectonically Active Setting: The New Madrid Seismic Zone.

Fabio Maselli, Claudio Conese, Ljiljana Petkov, and *Raffaello Resti,* Inclusion of Prior Probabilities Derived from a Nonparametric Process into the Maximum-Likelihood Classifier.

Ram M. Narayanan, Steven E. Green, and *Dennis R. Alexander,* Soil Classification Using Mid-Infrared Off-Normal Active Differential Reflectance Characteristics.

Kurt Novak, Rectification of Digital Imagery.

Laurent Polidori, Jean Chorowicz, and *Richard Guillande,* Description of Terrain as a Fractal Surface, and Application to Digital Elevation Model Quality Assessment.

Michael Rast, Simon J. Hook, Christopher D. Elvidge, and *Ronald E. Alley,* An Evaluation of Techniques for the Extraction of Mineral Absorption Features from High Spectral Resolution Remote Sensing Data.

Randall L. Repic, Jae K. Lee, Paul W. Mausel, David E. Escobar, and *James H. Everitt,* An Analysis of Selected Water Parameters in Surface Coal Mines Using Multispectral Videography.

Omar H. Shemdin and *H. Minh Tran,* Measuring Short Surface Waves with Stereophotography.

Thierry Toutin, Yves Carboneeau, and *Louiselle St-Laurent,* An Integrated Method to Rectify Airborne Radar Imagery Using DEM.

Zhuoqiao Zeng and *Xibo Wang,* A General Solution of a Closed Form Space Resection.